Petroleum Science 23 (2026) 422–433

Contents lists available at ScienceDirect

Petroleum Science

journal homepage: www.keaipublishing.com/en/journals/petroleum-science

Original Paper

Interfacial plugging of shale microfractures using functionalized graphene oxide with high dispersion stability under harsh conditions

Dao-Xiong Li [a,b], Yang Bai [a,b,c,*], Cheng Wang [d], Na Su [e], Ling-Feng Wu [b], Deng Gu [b], Yu-Fen Zhai [b], Ping-Ya Luo [a,b,**]

[a] State Key Laboratory of Oil & Gas Reservoir Geology and Exploitation, Southwest Petroleum University, Chengdu, 610500, Sichuan, China
[b] Petroleum Engineering School, Southwest Petroleum University, Chengdu, 610500, Sichuan, China
[c] National Engineering Research Center of Oil & Gas Drilling and Completion Technology, Beijing, 102200, China
[d] College of Chemistry and Chemical Engineering, Southwest Petroleum University, Chengdu, 610500, Sichuan, China
[e] Tianfu Yongxing Laboratory, Chengdu, 610000, Sichuan, China

ARTICLE INFO

Article history:
Received 21 May 2025
Received in revised form
15 September 2025
Accepted 15 September 2025
Available online 20 September 2025

Edited by Yan-Hua Sun

Keywords:
Functionalized GO
Stable dispersion
Interfacial plugging
Nanoplugging agent
Shale microfractures

ABSTRACT

Shale gas development often suffers from wellbore instability due to microfractures in the formation, posing serious challenges to drilling safety and efficiency. This study presents a functionalized graphene oxide (GO-PAA) nanomaterial, prepared by grafting hydrophilic polyacrylic acid (PAA) chains onto GO surfaces to enhance dispersion stability under high salinity, elevated temperature, and wide pH conditions. The results indicate that GO-PAA effectively resists charge-shielding effects under conditions of high salinity, elevated temperature, and a wide pH range, significantly reducing the risk of particle aggregation. Even at high salt concentrations, the zeta potential remains below −32.8 mV, demonstrating good colloidal stability. Plugging performance was evaluated using simulated core experiments. GO-PAA formed a "band-aid" like barrier on shale microfracture surfaces, reducing permeability by up to 57.53%, nearly twice that of conventional spherical nanoparticles. Scanning electron microscope (SEM) and elemental analysis confirmed the formation of a dense and uniform plugging layer. The synergistic interaction between GO's 2D lamellar structure and the flexible polymer chains facilitated effective surface adhesion and coverage. This adsorption–adhesion plugging mechanism represents a shift from traditional bridging theories, enabling reduced material usage and improved efficiency. The findings provide theoretical and practical support for designing high-performance nanoplugging agents in water-based drilling fluids, contributing to safer and more sustainable shale gas development.

1. Introduction

Currently, the global energy landscape is undergoing a critical transition from traditional fossil fuels to renewable energy sources. As a cleaner fossil fuel with lower carbon emissions, natural gas has become a crucial "bridge" and "partner" in achieving the "carbon peak and carbon neutrality" goals (Li et al., 2022; Melikoglu, 2014; Zou et al., 2024). Shale gas, as one of the natural forms of natural gas, has gradually gained prominence in global energy supply (Armor, 2013; Li et al., 2024). However, shale formations contain numerous microfractures (<1 μm), and drilling fluid, known as the "lifeblood" of drilling operations, not only supports the wellbore but also plays key roles in cleaning, cooling, and lubrication (Abdullah et al., 2022; Jiang et al., 2021; Zhao et al., 2019). During the drilling of shale formations, drilling fluids and their filtrates are highly prone to invading the formation, leading to wellbore instability and, consequently, economic losses (Chen et al., 2023; Liu et al., 2023; Wei et al., 2023; Zhou et al., 2024). According to statistics from the U.S. oil and gas industry, the total losses caused by wellbore instability and wellbore stability issues are approximately $5 billion, not including losses from other catastrophic events such as blowouts and environmental contamination (Jiang et al., 2021; Yang et al., 2016). To plug formation microfractures, the addition of nanoplugging agents in

* Corresponding author.
** Corresponding author.
E-mail addresses: 2014990101000@swpu.edu.cn (Y. Bai), luopy@swpu.edu.cn (P.-Y. Luo).
Peer review under the responsibility of China University of Petroleum (Beijing).

https://doi.org/10.1016/j.petsci.2025.09.030

drilling fluids can effectively plug shale formation microfractures, preventing the invasion of drilling fluids and their filtrates into the formation. This is critical for the safe and efficient development of shale gas.

Early researchers introduced widely sourced and low-cost inorganic nanoparticles, such as SiO_2, $CaCO_3$, and metal oxides, into drilling fluids as nanoplugging agents. However, the use of these materials in drilling fluids often results in aggregation and precipitation. Additionally, most of these nanoparticles are spherical, and based on the principle of tight packing, they accumulate endlessly within shale microfractures, effectively plugging them but requiring a large volume of material in the drilling fluid (Cai et al., 2012; Asma et al., 2021; Bai et al., 2024; Moslemizadeh and Shadizadeh, 2015; Toscano et al., 2016). Organic nanoparticles possess excellent elastic deformation properties, enabling dense plugging of shale microfractures, thus gaining considerable attention from researchers. However, in high-temperature and high-mineralization environments, organic nanoparticles suffer from poor thermal stability and low mechanical strength, making them prone to degradation or failure during high-temperature drilling operations, which in turn affects their plugging performance (An et al., 2023; Liu et al., 2015; Xie et al., 2015). In recent years, both domestic and international researchers have attempted to effectively combine inorganic and organic components to explore composite nanoplugging agents with improved plugging performance. However, the inorganic and organic components of these composites may exhibit different chemical or physical behavior in high-temperature, broad pH environments, leading to a decline in the overall material performance, particularly in high-temperature conditions, which impacts the plugging ability. Additionally, the preparation process of composite materials is complex, requiring high technical standards and making large-scale production difficult, thus limiting their industrial application (An et al., 2016; Jain et al., 2015; Wu et al., 2017). In light of the above challenges, the question arises whether it is possible to develop a simple and efficient preparation method for nanomaterials that are feasible for large-scale production. Such materials should maintain excellent stable dispersion properties under high-temperature, high-mineralization, and broad pH conditions. Furthermore, they should not penetrate shale microfractures upon addition to the drilling fluid, effectively plugging the fractures to reduce the amount of nano-materials used, thus addressing wellbore instability issues during shale gas drilling.

Compared with conventional nanoparticles, 2D nanomaterials exhibit ultrathin thickness and large lateral dimensions. This raises the possibility of endowing them with interfacial adhesion capabilities, allowing them to attach to shale microfracture surfaces like a “band-aid” and thereby prevent the infiltration of drilling fluids and their filtrates into the formation. Such a mechanism not only overcomes the limitations of traditional nanoparticles, which rely solely on continuous accumulation for fracture plugging, but also addresses the root cause of wellbore instability induced by filtrate invasion during shale gas drilling. The discovery of graphene in the early 21st century marked a historic breakthrough in the study of 2D nanomaterials, owing to its unique structure and excellent physicochemical properties (Huang et al., 2018). 2D nanomaterials have demonstrated immense potential in fields such as electronics, energy storage, catalysis, and biomedicine, driving revolutionary developments in science and technology (Novoselov et al., 2004; Verma and Yadav, 2024; Wang et al., 2024). Among these 2D nanomaterials, GO, a derivative of graphene, has become a research hotspot in recent years due to its rich surface functional groups and excellent chemical reactivity (Arun et al., 2024; Cao et al., 2024). However, GO also has certain limitations as a nanoplugging agent for water-based drilling fluids. Firstly, although GO surfaces contain hydrophilic functional groups that can interact with water molecules, the electrostatic and van der Waals interactions between GO particles may still lead to aggregation under high concentration and long-term storage conditions (Jiříčkováet et al., 2022). Secondly, in high-temperature environments such as shale formations, the oxygen-containing functional groups on the surface of GO may undergo thermal degradation or chemical changes, leading to a decrease in its dispersion stability (Chen et al., 2022; Lee et al., 2024). Additionally, shale formations are typically in high-mineralization environments, where ions in the water molecules compress the charge layer on the surface of GO, weakening its interaction with water. This results in particle aggregation, which negatively impacts the plugging performance (Pandey and Sharma, 2024; Pedico et al., 2024; Tang et al., 2024; Zhang et al., 2024). Therefore, to improve the stability, dispersion, and plugging performance of GO in drilling fluids, it is essential to modify its dispersion properties and structure, enhancing its effectiveness in complex environments.

This study presents a simple and scalable preparation method for functionalized GO composite materials, aiming to impart excellent adaptability under high temperature, high salinity, and wide pH conditions. Furthermore, molecular dynamics (MD) simulations were used to further validate the stable dispersion ability of the nanoparticle dispersion system. Based on this, the plugging performance of the functionalized GO composite material in shale gas formations was evaluated through “simulated core” experiments. Additionally, various characterization techniques, such as SEM and elemental analysis, were used to deeply investigate the plugging mechanism, revealing the important contribution of the synergistic effect between the 2D sheet structure and modified polymer chains in fracture plugging. This research provides an innovative solution for water-based shale gas drilling fluid systems, offering a simple preparation process with both efficient plugging ability and environmentally friendly characteristics. It aims to overcome the technical bottlenecks caused by wellbore instability during shale gas formation development, and to promote the practical engineering application of functionalized 2D nanomaterials in drilling fluids.

2. Experimental section

2.1. Materials

GO was synthesized in the laboratory following the Hummers' method (material characterization is shown in Figs. S1 and S2). *N*, *N*-dimethylacetamide (DMAc), 4,4′-diaminodiphenyl ether (ODA), pyromellitic dianhydride (PMDA), sodium carbonate (Na_2CO_3), and nano-calcium carbonate (nano-$CaCO_3$, 300 nm) were obtained from Beijing Yan Cheng Technology Co., Ltd.; bentonite (BT), sulfonated lignite (SMC), sulfonated phenolic resin (SMP-II), and barite ($BaSO_4$) were obtained from Sichuan Shida Jinniu Technology Co., Ltd. All chemicals were used as received.

2.2. Material characterization

Fourier-transform infrared spectroscopy (FT-IR, Thermo Fisher Scientific Nicolet iS20) was used to identify the functional groups of GO and GO-PAA, with a testing range of 4000 to 400 cm^{-1}. This was performed to observe the changes in characteristic absorption peaks such as carboxyl group (–COOH), hydroxyl group (–OH), and amide group (N–C=O) before and after PAA grafting. X-ray

photoelectron spectroscopy (XPS, Thermo Scientific K-Alpha) was used to examine the surface chemical structure of GO and GO-PAA. Monochromatic Al Kα radiation (1486.6 eV) was employed to analyze the elemental composition of the sample surfaces in a vacuum environment. Transmission electron microscopy (TEM, JEOL JEM-2100, Japan) was used to observe the microscopic morphology of GO and GO-PAA at an accelerating voltage of 200 kV. The samples were prepared by allowing drops of ultrasonic dispersion to naturally evaporate on copper grid carbon films. Atomic force microscopy (AFM, Bruker Multi Mode 8) was used to measure the thickness changes of the samples. Tapping mode was employed to scan the thickness differences at the edges of GO and GO-PAA samples to determine the increase in thickness after modification.

2.3. Performance testing

2.3.1. Stability and dispersion performance

The hydrophilicity of the sample surfaces was evaluated through the contact angle test using a contact angle measuring instrument (Data Physics OCA Series). A 2 μL droplet of pure water was automatically applied, and the contact angles of GO and GO-PAA were measured to analyze the changes in hydrophilicity before and after PAA grafting on the GO surface. Thermogravimetric analysis (TG-DSC, Mettler TGA/DSC1) was used to determine the organic content and thermal stability of GO and GO-PAA. The samples were tested in the range of 40–800 °C at a heating rate of 10 °C/min, and the mass loss was analyzed to study the impact of PAA modification on the thermal decomposition behavior of GO. The zeta potential reflects the surface charge density of particles and their ability to attract surrounding ionic layers, serving as a key indicator of colloidal dispersion stability. It is generally accepted that when the absolute value of the zeta potential exceeds 30 mV, sufficient electrostatic repulsion exists between particles to prevent aggregation and maintain good dispersion. To evaluate the effect of PAA grafting on the dispersion stability of GO, a zeta potential analyzer (Malvern Zeta Sizer Nano ZS) was used to measure the zeta potential of both GO and GO-PAA under varying pH conditions (5–9) and different salt concentrations (10,000, 50,000, and 100,000 ppm). The salt solutions were prepared by dissolving NaCl and $CaCl_2$ at a 1:1 mass ratio in deionized water to simulate the influence of highly mineralized environments on dispersion performance (Bhattacharjee, 2016; Huang et al., 2023). The mixed monovalent cation (Na^+) and divalent cation (Ca^{2+}) were used to simulate the actual mineralized water environment present in shale formations. Divalent cations exert a more significant effect on the electric double layer compression, providing a more realistic representation of the material's dispersion behavior under complex formation conditions. In addition, the dispersion of GO and GO-PAA in deionized water was observed visually. The dispersion was placed in a static container and left to stand at 120 °C for 48 h. The uniformity and sedimentation status were then observed to evaluate the improvement effect of PAA modification on dispersion.

2.3.2. MD simulation

MD simulations were used to study the molecular structure and interactions of GO and GO-PAA. The models of GO and GO-PAA were constructed using Materials Studio (Figs. S4 and S5). The Gaussian 16 program was used to optimize the four side-chain structures of GO-PAA using the B3LYP-D3 functional and 6-31G(d) basis set. The force field parameters for GO were derived from previous studies (Almarzooqi et al., 2024). Full-atom MD simulations were performed using the GROMACS software package (version 2021.5), employing the OPLSAA force field and the SPC/E water model to describe the molecules. In the simulation, 20 GO molecules were randomly inserted into a 10 nm × 10 nm × 10 nm cubic box, filled with water molecules, and Na^+, Ca^{2+}, and Cl^- ions were added to simulate the dispersion behavior of GO at a salt concentration of 50,000 ppm, thereby constructing a pure GO simulation system. The construction of the GO-PAA simulation system was similar to that of the GO simulation system, but its cubic box size was 15 nm × 15 nm × 15 nm. To avoid large influences of the molecules on the simulation results, both systems were simulated and processed in subsequent MD simulations. After energy minimization using the steepest descent method, short 500 ps simulations were carried out using the NVT and NPT ensembles. Subsequently, the NPT ensemble was used for data generation over a period of 50 ns. During the simulation, the Parrinello–Rahman barostat was used to maintain a pressure of 1.0 bar, and a velocity-rescaling thermostat with a coupling constant of $\tau = 0.1$ ps was used to control the temperature at 298.15 K. Non-bonded interactions were calculated with a cutoff value of 1.2 nm, and long-range electrostatic interactions were computed using the particle mesh Ewald summation method. All hydrogen bond constraints were implemented using the linear constraint solver (LINCS) algorithm, with a simulation step size of 2 fs and neighbor lists updated every 10 steps. Periodic boundary conditions were applied in all three directions. Finally, molecular visualization was performed using PyMOL-3.0.3 (http://www.pymol.org/pymol) to analyze the stable dispersion ability of GO and GO-PAA systems in formation environments. To further quantify their aggregation behavior, we calculated the radial distribution function (RDF) of a single randomly chosen GO or GO-PAA molecule with the other 19 nanosheets during the 40–50 ns equilibrium phase of the system. The RDF is one of the most important functions in describing the structure of fluids, and its definition is given by Eq. (1):

$$g_{\alpha\beta}(r) = \frac{1}{4\pi\rho_\beta r^2}\left[\frac{dN_{\alpha\beta}(r)}{dr}\right] \quad (1)$$

where ρ_β is the number density of β particles; $N_{\alpha\beta}(r)$ represents the average number of β particles within a sphere of radius r centered around an α particle. The peaks of the RDF reflect the binding strength and local density between particles. The higher the peak, the stronger the binding and the higher the local density.

2.3.3. Plugging performance

Shale, as one of the most typical low-permeability rocks, usually has a very low permeability, typically below 10^{-3} mD, with some shales reaching nanoscale levels (Hu et al., 2024; Safaei and Tavakoli, 2017). To test the plugging ability of nanomaterials on microfractures in shale formations, a "simulated core" was prepared to mimic low-permeability shale. The plugging performance of the nanomaterials was evaluated by the reduction in permeability, microscopic morphology, and changes in elemental composition before and after plugging in the "simulated core".

2.3.3.1. Preparation method of the "simulated core"

(1) Preparation of the experimental slurry: Under high-speed stirring conditions, BT (6%) and Na_2CO_3 (0.3%) were sequentially added to deionized water at 75 °C, stirred, and sealed to rest for 24 h. Under low-speed stirring conditions, SMC (5%), SMP-II (5%), and $BaSO_4$ (10%) were successively added, ensuring uniform dispersion of each additive. After all components were added, the slurry was transferred to a high-speed stirring cup and mixed for an additional 20 min. Finally, the slurry was aged at 105 °C for 16 h to prepare the experimental slurry for the "simulated core".

(2) A high-temperature, high-pressure filtration experiment was conducted using a high-temperature high-pressure filtration apparatus, as shown in Fig. S6, under conditions of 105 °C and 3.5 MPa. After the experiment, the high-temperature high-pressure filtration apparatus was cooled to room temperature, and the "simulated core" was removed. Deionized water was used to wash off the residual experimental slurry from the surface of the "simulated core" to obtain the "simulated core". The "simulated core" was placed back into the filtration apparatus, and deionized water was passed through the "simulated core" at a pressure differential of 3.5 MPa and a temperature of 105 °C. During the experiment, after applying pressure, the filtrate was immediately collected, and then filtrate was collected every 5 min. The volume of the filtrate was recorded until the experiment ended after 30 min. After the experiment, the apparatus was cooled to room temperature, and the "simulated core" was removed. Using a vernier caliper, the thickness of the "simulated core" was measured at multiple randomly selected points on its surface, and the average value was calculated as the thickness of the "simulated core".

The original permeability k_0 of the "simulated core" was calculated using Darcy's law, as shown in Eq. (2):

$$k = \frac{Q\mu L}{A\Delta P} \tag{2}$$

where k is the permeability of the "simulated core", mD; Q is the filtration rate, and the volume of the collected filtrate versus time is used to obtain a straight line with a slope corresponding to the Q value, cm^3/s; μ is the viscosity of the filtrate at 25 °C, 1 cP; L is the thickness of the mud cake, mm; ΔP is the total pressure drop, 3.5 MPa; A is the cross-sectional area through which the fluid flows, 23.8 cm^2.

2.3.3.2. Evaluation of plugging performance. Based on the preparation of the "simulated core", the plugging performance of nanomaterials for microcracks in shale formations was investigated. Nano-dispersion liquids with different mass concentrations (0.25%, 0.50%, and 0.75%) were prepared. The nano-dispersion liquids were then added to the high-temperature, high-pressure filtration apparatus, where they were passed through the "simulated core" under a pressure differential of 3.5 MPa and a temperature of 105 °C. During the experiment, the filtrate was immediately collected after pressurization, and then filtered every 5 min, with the volume recorded until the experiment was terminated after 30 min. After the experiment, the apparatus was removed and cooled to room temperature. The "simulated core" was then extracted from the apparatus and cleaned of any remaining nano-dispersion liquid. Using a caliper, multiple random points on the surface of the "simulated core" were measured for thickness, and the average value was calculated to determine the thickness of the "simulated core". The permeability (k_1) of the "simulated core" after treatment with the nano-dispersion liquid was also calculated using Eq. (2). Therefore, the permeability reduction rate (K_r) of the "simulated core" after the addition of the nano-dispersion liquid was calculated using Eq. (3):

$$K_r = \frac{k_0 - k_1}{k_0} \times 100\% \tag{3}$$

where K_r represents the permeability reduction rate of the "simulated core" after treatment with the nano-dispersion liquid; k_0 denotes the original permeability of the "simulated core", mD; k_1 is the permeability of the "simulated core" after treatment with the nano-dispersion liquid.

The surface morphology of the "simulated core" before and after treatment with the nano-dispersion liquid was observed using a scanning electron microscope (SEM, Hitachi SU8010). The tests were conducted under high vacuum mode with an acceleration voltage of 15 kV, to analyze the blockage structure formed by the nano-dispersion liquid on the crack surface, as well as the density and uniformity of the blockage layer. Energy-dispersive X-ray spectroscopy (EDS, Oxford X-Max 20) was used in conjunction with SEM to analyze the elemental composition of the surface of the "simulated core" after treatment. After GO-PAA blocking, the distribution of C and O elements was primarily analyzed to verify that the GO-PAA sheets mainly stayed on the crack surface. For the samples treated with nano-dispersion of $CaCO_3$, the distribution of Ca element was primarily analyzed to assess the blocking mechanism through particle physical filling. By comparing the distribution of elements on the surface and cross-section, the unique mechanism of interaction between GO-PAA and the crack surface during the blocking process was further investigated.

3. Results and discussion

3.1. Preparation of GO-PAA

As shown in Fig. 1(a), the nanocomposite material GO-PAA was prepared using a two-step process. In the first step, under nitrogen (N_2) protection as shown in Fig. 1(b), ODA and PMDA were dissolved in a DMAc solution, and a specific amount of catalyst was added to promote the polycondensation reaction, resulting in a PAA solution. In the second step, under N_2 protection, the PAA solution was blended with GO, and an initiator and catalyst were added to facilitate the chemical reaction between the –COOH and N–C=O of PAA and the oxygen-containing functional groups (such as –COOH and –OH) on the GO surface, forming stable chemical bonds and ultimately generating the GO-PAA as shown in Fig. 1(c), with a median particle size of 321 nm (Fig. S3).

Fig. 1(d) shows infrared spectra of GO and GO-PAA. The GO-PAA, grafted with PAA, shows absorption peaks at 1576 and 1227 cm^{-1}, corresponding to the characteristic peaks of N–H and C–N bonds in the N–C=O, confirming the presence of the N–C=O. The absorption peak at 1736 cm^{-1} represents the C=O characteristic peak in the N–C=O, indicating the success of the amide reaction. These data confirm the successful grafting of PAA on the GO surface.

Fig. 1(e) shows full XPS spectra of GO and GO-PAA. The spectra indicate the presence of nitrogen (N) in GO-PAA, which is absent in the GO spectrum. The N element originates from the PAA. Additionally, as shown in Fig. 1(f), the C 1*s* peak of GO-PAA was deconvoluted into five peaks at 284.3 eV (C–C), 285.2 eV (C–N), 286.7 eV (C–O), 287.7 eV (N–C=O), and 288.2 eV (C=O). The peak at 287.8 eV corresponds to the binding energy of the –N–C=O in the N–C=O. Moreover, as shown in Fig. 1(g), the N 1*s* spectrum of GO-PAA was also fitted, revealing two peaks with binding energies at 399.6 and 401.2 eV. After grafting with the initiator, a new peak appeared at 399.6 eV, representing the binding energy of nitrogen in the N–C=O, further confirming the successful grafting of PAA onto the GO surface through the amide reaction, resulting in the GO-PAA.

As shown in Fig. 2(a), GO exhibits a typical 2D layered structure, with some wrinkles and stacking at the edges. This structure results

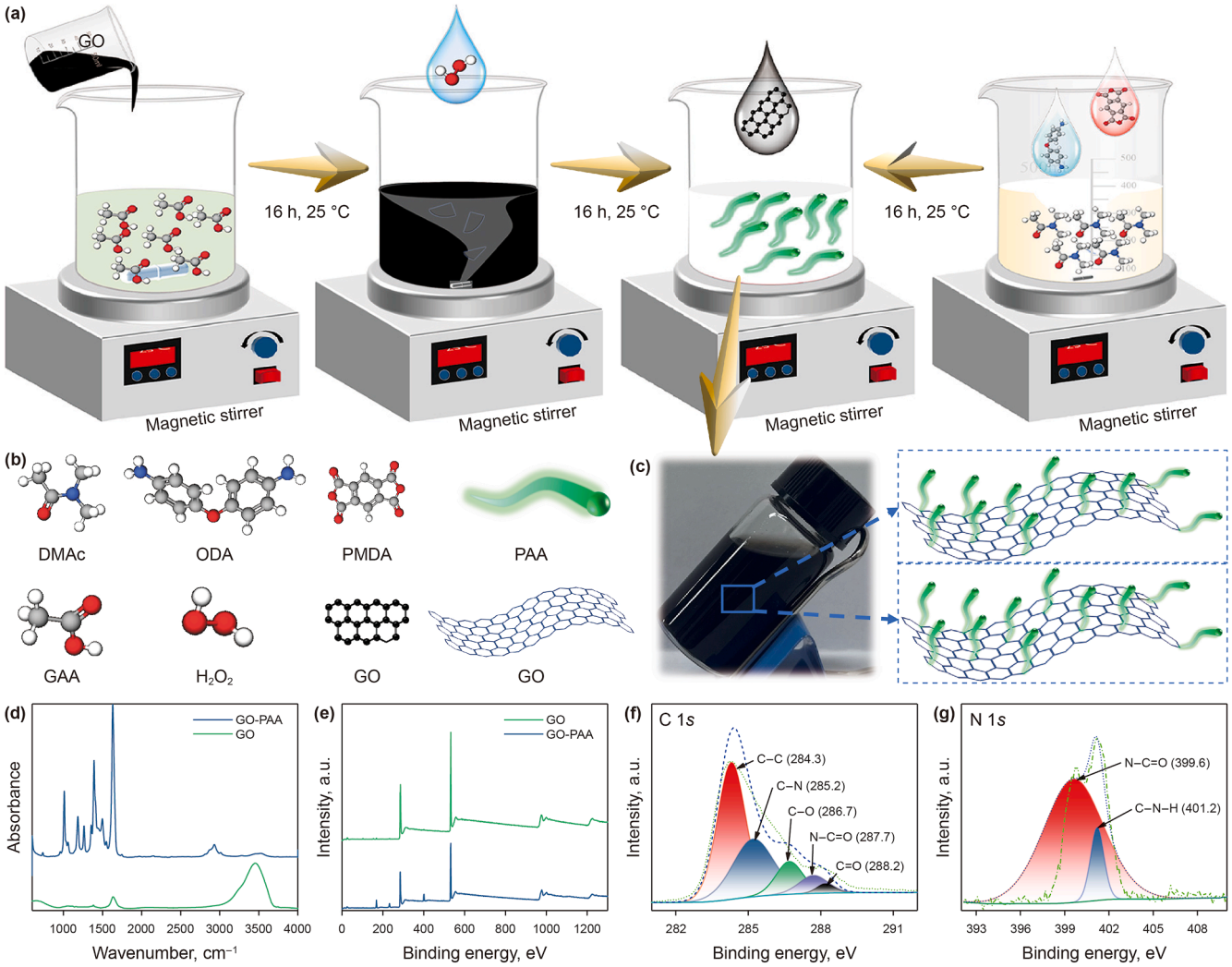

Fig. 1. Preparation process and material characterization of GO-PAA. (**a**) Preparation process of GO-PAA. (**b**) Schematic of the chemicals and products used during the preparation of GO-PAA. (**c**) GO-PAA product. (**d**) Infrared spectra of GO and GO-PAA. (**e**) Full spectra of GO and GO-PAA. (**f**) C element peak fitting. (**g**) N element peak fitting.

from the van der Waals forces between the GO sheets. After grafting PAA onto its surface, a large number of chain-like structures are observed on the GO surface in Fig. 2(b) due to sample deposition, confirming the chain morphology of the grafted polymer. The TEM images further confirm the successful grafting of PAA molecules, which not only significantly enhances the surface chemical reactivity of GO but also improves its hydrophilicity and dispersion in aqueous systems by forming long-chain structures. This modification technique significantly improves the hydrophilicity and environmental adaptability of GO, laying a solid foundation for its practical application as an efficient plugging material in drilling fluids.

Fig. 2(c) and (d), as observed through AFM analysis, further reveal the morphological changes before and after the grafting of PAA molecules onto the GO surface. After PAA was grafted onto the GO surface, chain-like or protruding structures appeared at the edges of the layers, reflecting the uniform distribution and successful attachment of PAA molecular chains on the GO surface. Additionally, as shown in Fig. 2(e) and (f), the thickness of GO is primarily around 2 nm, indicating that it consists of few-layer graphene oxide and exhibits a good 2D layered structure. The thickness of the GO-PAA sample increased to 3 nm after PAA grafting, which is attributed to the attachment of PAA chains to the GO surface. This increase in thickness not only verifies the success of the grafting modification but also indicates that the modified GO-PAA possesses greater physical structural stability.

3.2. Stability and dispersion performance of GO-PAA

Through contact angle measurements, thermogravimetric analysis (TGA), and zeta potential characterization, we explored the application potential of the GO-PAA in water-based drilling fluids. The contact angle measurements indicate that the contact angle of GO shown in Fig. 3(a) is 41.67°, while the contact angle of the GO-PAA grafted with PAA, as shown in Fig. 3(b), significantly decreases to 10.51°, indicating a substantial increase in the hydrophilicity of GO-PAA. This change is mainly attributed to the introduction of hydrophilic functional groups, such as –COOH and –OH, on the PAA molecular chains, which significantly enhance the interaction between GO-PAA and water molecules. Additionally, the flexible structure of the PAA molecular chains covers the surface of the GO sheets, creating a more uniform hydrophilic interface, thereby significantly reducing the contact angle (Zhao et al., 2025). The enhanced hydrophilicity makes GO-PAA more easily dispersed and stable in water-based drilling fluids, which is crucial

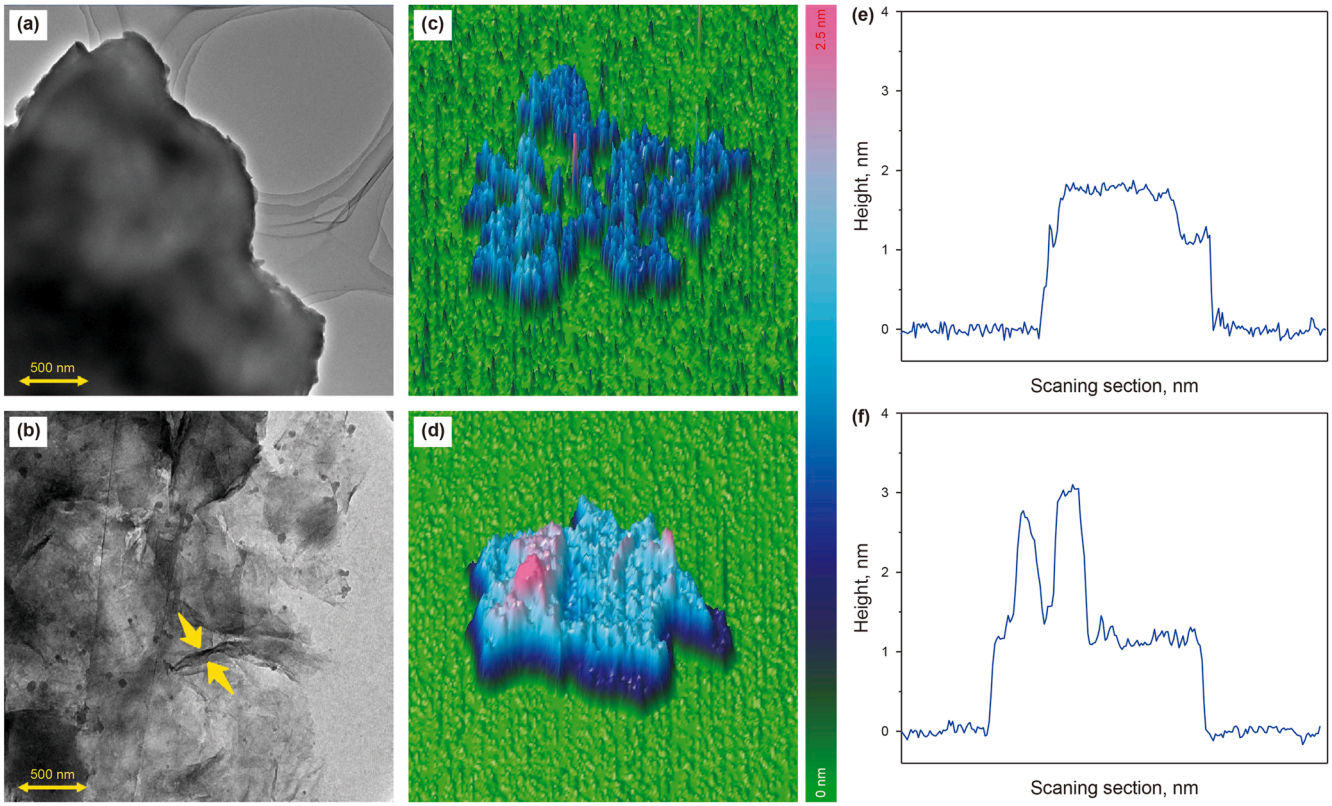

Fig. 2. TEM images of GO (**a**) and GO-PAA (**b**). AFM images of GO (**c**) and GO-PAA (**d**). Thicknesses of GO (**e**) and GO-PAA (**f**).

for improving its plugging performance in complex strata environments.

A comparison of the TGA results of GO and GO-PAA reveals a significant enhancement in the thermal stability of GO after PAA grafting. As shown in Fig. 3(c), the mass loss of GO is primarily concentrated in the rage of 100–200 °C, attributed to the thermal desorption of surface oxidized groups such as –COOH and –OH, accompanied by the release of water molecules and carbon dioxide. In 300–500 °C, the carbon backbone of GO further decomposes, leading to a significant increase in the mass loss rate, which limits its application under high-temperature conditions. In contrast, as shown in Fig. 3(d), GO-PAA exhibits only a slight mass loss around 150 °C, primarily due to the desorption of some free groups from the PAA molecular chains, indicating that PAA grafting effectively reduces the desorption of active groups at low temperatures. Moreover, as the temperature increases, the mass loss rate of GO-PAA significantly slows down, indicating that the introduction of PAA molecules delays the decomposition of the carbon backbone due to their high-temperature stability and long-chain structure. The enhanced effect of PAA grafting can be attributed to the thermal protective effect provided by the polymer chains and the stability of the chemical bonds, which significantly improve the overall thermal stability of the material (Yu et al., 2024). In summary, PAA grafting not only imparts higher surface chemical activity to GO but also enhances its structural integrity under high-temperature conditions, significantly improving the application potential of GO-PAA in complex strata environments and providing theoretical support and performance assurance for its application in water-based drilling fluids.

Zeta potential analysis indicates that the surface charge of GO-PAA exhibits significant dynamic responses to changes in pH and salt concentration. As shown in Fig. 3(e), under different pH conditions, the zeta potential of GO-PAA gradually increases as the pH value rises from 5 to 9, primarily due to the dissociation behavior of the surface –COOH after PAA grafting. Under acidic conditions, the –COOH groups do not fully dissociate and remain in their neutral form, resulting in a lower surface negative charge density; whereas, under alkaline conditions, the –COOH largely dissociate into negative charges (–COO–), significantly enhancing the electrostatic repulsion between particles, thus improving the dispersion and stability of GO-PAA in alkaline environments (Hu et al., 2024; Yagura et al., 2021). Additionally, the extension of the flexible PAA chains not only provides a steric hindrance effect, effectively preventing particle aggregation, but also further amplifies the change in zeta potential through the stability of the electrical double layer. This dual effect significantly improves the dispersion performance of GO-PAA under alkaline conditions. However, as the salt concentration increases from 10,000 to 100,000 ppm, the zeta potential of GO-PAA gradually decreases, reflecting the effect of the charge screening in high salinity environments on GO-PAA. Under high salinity conditions, the cations in the solution neutralize the negative charge on the GO-PAA surface and compress the electrical double layer on the particle surface, leading to a reduction in electrostatic repulsion between particles, thereby increasing the likelihood of particle aggregation. However, the presence of the flexible PAA chains plays a significant buffering role in this process. The steric hindrance effect of the PAA chains, along with the interaction between its polar groups and cations, effectively reduces direct contact between particles, thereby partially offsetting the negative impact of increased salt concentration on dispersion (Sawada and Nogami, 2004). Therefore, despite the decrease in zeta potential at high salinity concentrations, the surface charge of GO-PAA remains below −30 mV, which is sufficient to ensure its dispersion stability in water-based

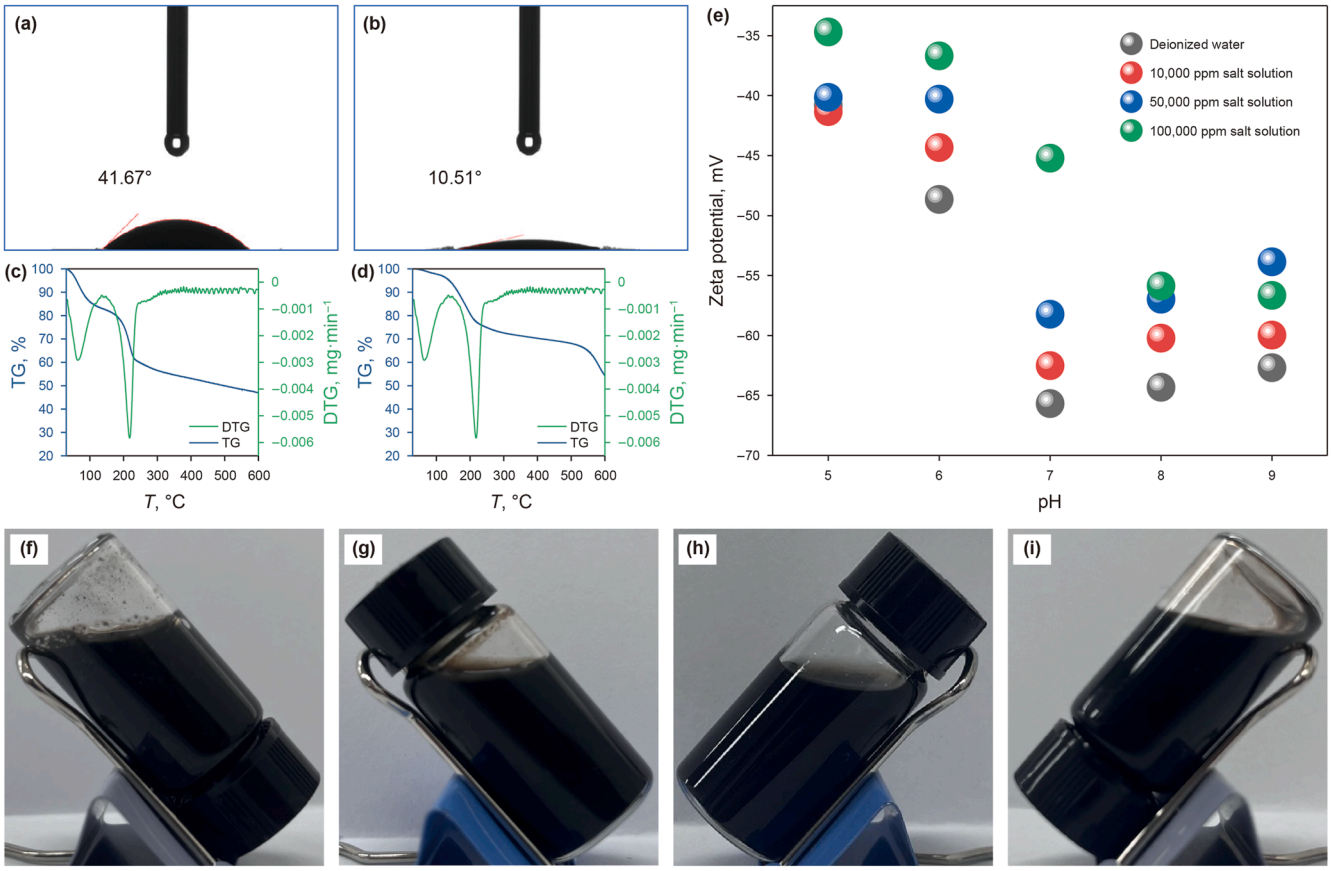

Fig. 3. Contact angles of GO (**a**) and GO-PAA (**b**). Thermogravimetric curves of GO (**c**) and GO-PPA (**d**). (**e**) Zeta potential values of GO-PAA under different pH and salt concentration conditions. Top view (**f**) and front view (**g**) of GO dispersion. Front view (**h**) and top view (**i**) of GO-PAA dispersion.

drilling fluids, indicating that it can still meet the application requirements under high salinity conditions.

After being placed at 120 °C for 48 h, the GO dispersion and GO-PAA dispersion show significant differences in the top view (Fig. 3 (f) and (i)), while no significant differences are observed in the front view (Fig. 3(g) and (h)). From the top view, it can be observed that after high-temperature exposure, the GO dispersion undergoes significant sedimentation, with particles concentrated at the bottom of the bottle, indicating poor stability under high-temperature conditions, where the weakening of electrostatic repulsion between particles leads to aggregation. In contrast, the top view of the GO-PAA dispersion shows that even after 12 h of high-temperature exposure, its particles remain suspended without significant sedimentation. This difference is attributed to the grafting effect of the PAA chains, which effectively suppress particle aggregation and sedimentation through the hydration layer and electrostatic repulsion of the flexible chains. The results indicate that the dispersion performance of GO-PAA under high-temperature conditions is significantly better than that of unmodified GO, providing reliable evidence for its application in high-temperature environments.

Combining the experimental results of contact angle, TGA, and zeta potential, the excellence of GO-PAA is attributed to its unique microstructure and surface chemical characteristics. PAA grafting not only enhances the hydrophilicity and dispersion of GO but also significantly improves its functionalization ability in water-based drilling fluids. The chain structure of the grafted PAA effectively blocks microfractures in shale formations, preventing the intrusion of drilling fluid and filtrate, thereby improving the stability of the wellbore. Although the charge shielding effect under high salinity concentrations may impact the dispersion of GO-PAA, through reasonable formulation adjustments and further modification measures, GO-PAA can still exhibit outstanding performance in high-temperature, high-salinity, and wide pH environments.

3.3. MD simulation

The MD simulation results from Fig. 4 and videos (Multimedia components 1 and 2) clearly show significant differences in the dispersion behavior of GO and GO-PAA in the system. By comparing the structural evolution of the two systems over different time scales, we can draw the following conclusions. In the GO simulation system (Fig. S7 and Fig. 4(a)), the GO sheets are initially evenly dispersed in the system. However, as time progresses (10–50 ns), the GO sheets quickly undergo direct stacking and ultimately form dense aggregates. The enlarged image at 50 ns (Fig. 4(a)) shows that the GO nanosheets are primarily held together through van der Waals forces and π-π stacking interactions, forming sheet aggregates. This rapid aggregation indicates that the interactions between the GO sheets are strong, making it difficult for them to maintain a stable dispersion in the solution. In contrast, the GO-PAA simulation system (Fig. S8 and Fig. 4(b)) exhibits better dispersion throughout the simulation process. At 0 ns, the GO-PAA sheets are similarly dispersed evenly within the system, like the GO system. However, during the period of 10–50 ns, the GO-PAA system maintains a better dispersion state, and compared to the GO system, the aggregation between its

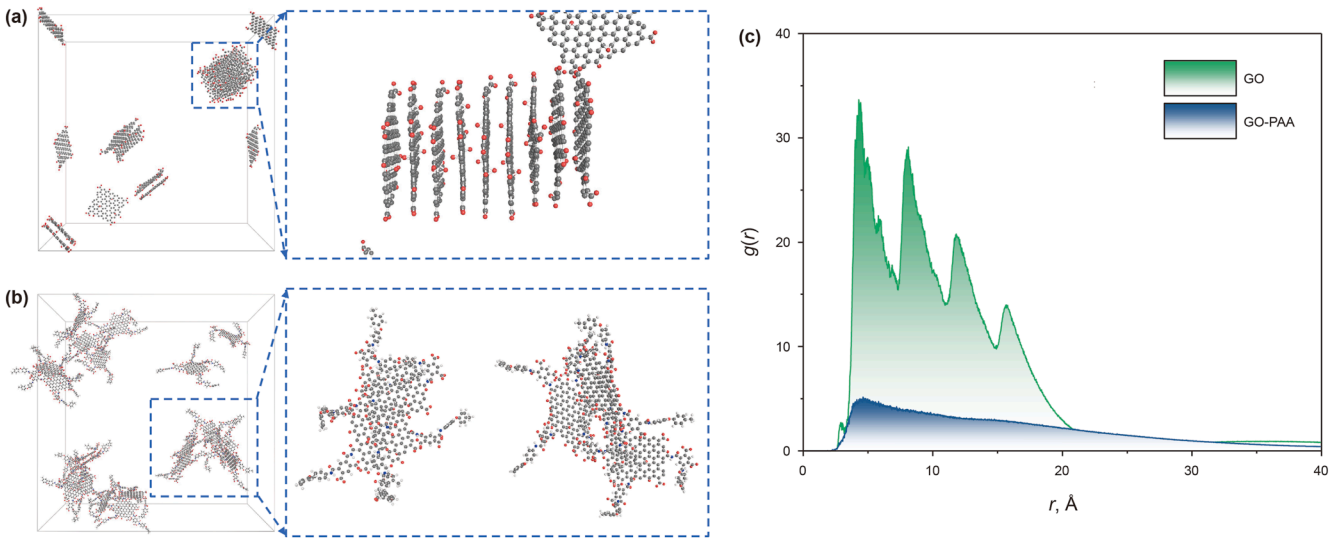

Fig. 4. Magnified views of GO (**a**) and GO-PAA (**b**) simulation systems at 50 ns. (**c**) RDF and coordination number of a randomly selected single GO and GO-PAA with 19 other nanosheets during the simulation period of 40–50 ns.

sheets is significantly reduced. The enlarged image at 50 ns (Fig. 4 (b)) shows that a more dispersed network structure forms between GO-PAA, rather than the tight stacking of sheets seen in the GO system. This suggests that the grafting of PAA effectively disrupts the strong interactions between the GO sheets, improving their dispersion stability.

RDF analysis further validates the dispersion advantage of the GO-PAA system. RDF is an important metric for measuring the particle interactions and structural characteristics in fluid systems, with the height of its peaks reflecting the binding strength and local density between particles. As shown in Fig. 4(c), the RDF peak of the GO system is higher, indicating stronger interactions between the GO sheets, resulting in a higher density of aggregates. This indicates that the GO system is prone to sheet stacking, making it difficult to maintain a well-dispersed state. In contrast, the RDF peak of the GO-PAA system is significantly lower than that of the GO system, indicating weaker binding forces between its sheets and reduced local density. This means that the grafting of PAA effectively reduces the attractive interactions between GO sheets, enhancing the dispersion of the system and reducing the formation of aggregates.

The differences in aggregation behavior between the GO and GO-PAA systems are primarily caused by the following factors. First, the π-π stacking interactions between GO sheets are strong, causing them to easily stack directly and form aggregates. However, in GO-PAA, the grafting of PAA molecules disrupts the π-π interactions, reducing the aggregation capability between GO sheets. Second, the introduction of PAA in GO-PAA leads to more negative charges on the surface of the sheets, enhancing electrostatic repulsion and thus reducing the binding strength between the sheets, which improves dispersion. Additionally, the PAA side chains in the GO-PAA system may form more hydrogen bonds with water molecules, enhancing the system's hydration capacity and making the GO-PAA sheets more stable in solution.

3.4. GO-PAA plugging performance

Through "simulated core" plugging performance tests, the plugging effectiveness of GO-PAA and nano-$CaCO_3$ was systematically evaluated (experimental data are shown in Table S1). As shown in Fig. 5(a)–(c), after adding 0.25%, 0.50%, and 0.75% nano-$CaCO_3$, the permeability reduction rates were 17.71%, 24.23%, and 25.49%, respectively. The plugging effect slightly improved with increasing concentration but tended to saturate. In contrast, as shown in Fig. 5(d)–(f), after adding 0.25%, 0.50%, and 0.75% GO-PAA, the permeability reduction rates significantly increased, reaching 44.15%, 54.41%, and 57.53%, demonstrating superior plugging performance. The filtration loss curves in Fig. 5 further indicate that the plugging effect of nano-$CaCO_3$ mainly relies on the physical filling effect of the particles. The filtration loss volume and rate decrease with increasing concentration, but the overall effect is limited by the compactness of particle packing and the irregularity of crack morphology. In contrast, GO-PAA demonstrated significantly better filtration loss control compared to nano-$CaCO_3$ at all concentrations, especially at 0.75% concentration, where the filtration loss volume and rate were at their lowest, being twice that of conventional materials. Its outstanding performance can be attributed to the unique 2D nanosheet structure of GO-PAA and the synergistic effect of the grafted PAA chains. The GO nanosheets can cover the crack surfaces, forming a "band-aid" barrier that effectively prevents the intrusion of drilling fluid and filtrate. The flexible PAA chains form a dense and stable plugging layer through physical filling and chemical adsorption. Additionally, the high hydrophilicity and chemical stability of PAA enhance the dispersion and environmental adaptability of GO-PAA in water-based drilling fluids, further improving the plugging performance (Ma et al., 2022).

The SEM results combined with elemental composition analysis reveal significant differences in the surface blocking performance of GO-PAA and nano-$CaCO_3$ on the "simulated core," providing clear evidence for the blocking mechanisms of the two materials. SEM images show no significant differences in the "simulated core" before treatment with either material (Fig. 6(a) and (d)). After treatment with GO-PAA, the surface structure of the "simulated core" is uniform and compact, indicating its ability to form a continuous and stable blocking layer (Fig. 6(e)). In contrast, the "simulated core" treated with nano-$CaCO_3$ exhibits loose particle aggregation, making it difficult to effectively fill cracks and pores. Its blocking ability is clearly limited by the simple physical filling effect of inorganic particles (Fig. 6(b)). Elemental composition analysis shows that significant Ca element signals are detected on both the surface and cross-section of the "simulated core" after treatment with nano-$CaCO_3$

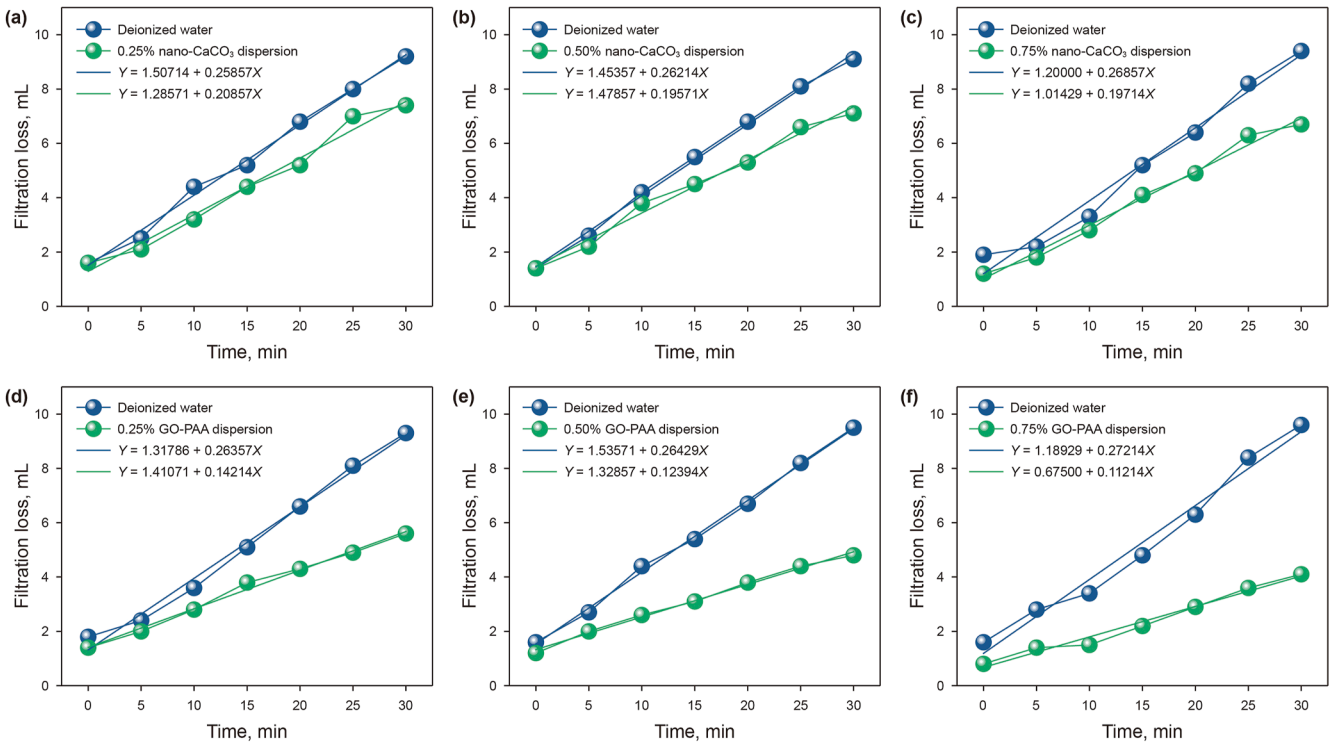

Fig. 5. The blocking effect of nano-dispersions on "simulated core". Filtration loss at different nano-$CaCO_3$ mass concentrations: (**a**) 0.25%, (**b**) 0.50%, (**c**) 0.75%. Filtration loss at different GO-PAA mass concentrations: (**d**) 0.25%, (**e**) 0.50%, (**f**) 0.75%.

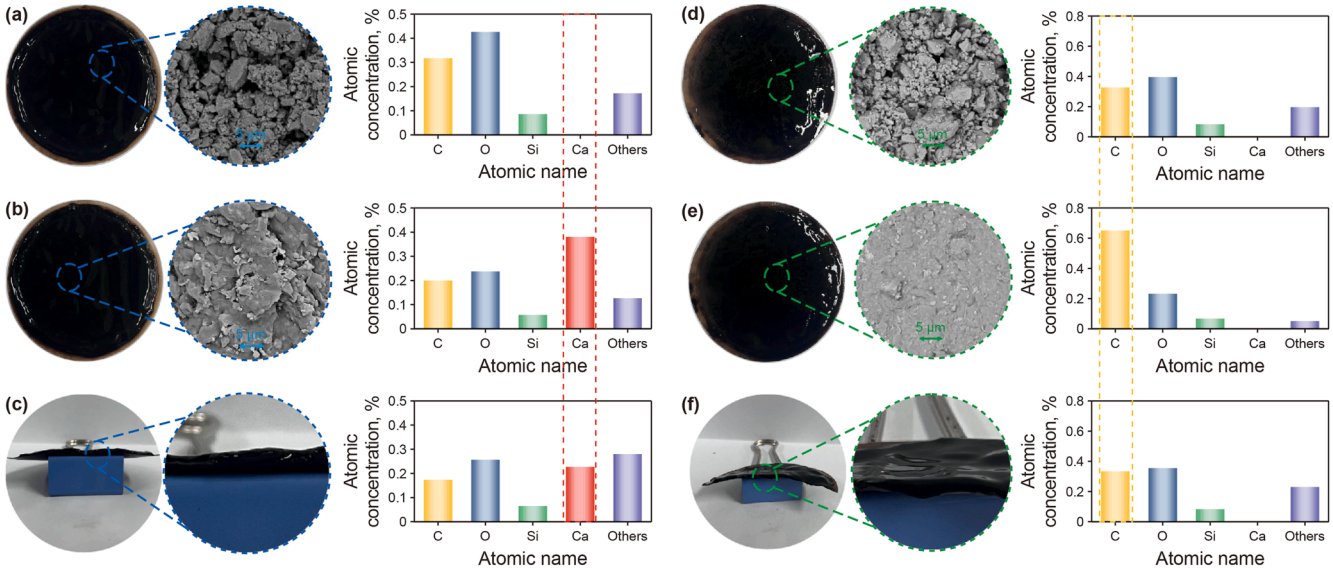

Fig. 6. Planar, SEM, and EDS analysis images of the "simulated core" before (**a**) and after (**b**) treatment with 0.75% nano-$CaCO_3$ nano-dispersion. Planar, SEM, and EDS analysis images of the "simulated core" before (**d**) and after (**e**) treatment with 0.75% GO-PAA nano-dispersion. Cross-sectional, magnified, and EDS analysis images of the "simulated core" after treatment with 0.75% nano-$CaCO_3$ nano-dispersion (**c**) and 0.75% GO-PAA nano-dispersion (**f**).

(Fig. 6(b) and (c)), further proving that the blocking mechanism of nano-$CaCO_3$ mainly relies on particle physical accumulation. However, this blocking method requires a large amount of material, and under conditions with high crack irregularity, the particle accumulation efficiency significantly decreases, leading to limited blocking performance. In contrast, the surface of the simulated core treated with GO-PAA shows a significant increase in the C element content, while the change in C element content on the cross-section is minimal, indicating that the blocking action of GO-PAA mainly occurs on the surface of the cracks (Fig. 6(d)–(f)). The layered structure of GO-PAA can cover the crack surface like a "band-aid", and its grafted PAA chains further enhance the material's adhesiveness, allowing it to adapt to the irregularities of the crack shapes. This results in efficient blocking through the synergistic effect of physical coverage and chemical adhesion. Furthermore, GO-PAA demonstrates excellent environmental adaptability. Under extreme conditions (such as high

mineralization, high temperature, and alkaline environments), GO-PAA can still maintain the bonding ability of its layered structure and the chemical stability of the PAA chains. This performance is derived from its layered-chain synergistic blocking mechanism. Compared to nano-$CaCO_3$, GO-PAA exhibits higher efficiency in blocking shale microcracks, providing an efficient and innovative material solution to address issues caused by wellbore instability during shale gas development.

3.5. Discussion on the blocking mechanism

The exceptional performance of GO-PAA composites in blocking shale microfractures stems from the synergistic effect of the 2D GO sheet structure and the surface-grafted PAA chains. The 2D sheet structure of GO has an extremely high specific surface area and flexibility, allowing it to cover the surface of shale microfractures like a "band-aid", blocking the intrusion of drilling fluids and filtrate through a physical barrier, while adapting to the irregular shapes of the fractures (Fig. 7). In contrast, the blocking effect of traditional spherical nanoparticles (such as $CaCO_3$, SiO_2, etc.) mainly relies on the physical filling of particles. Although their filtration loss decreases with increasing concentration of nano-dispersions, the overall effect is limited by the packing density of the particles and the irregularity of the fracture shapes, making it difficult to form a uniform, dense blocking layer in complex fractures. In contrast, GO-PAA overcomes these limitations through its unique 2D structure and surface modification.

Structurally, GO-PAA utilizes GO nanosheets as the framework, characterized by large lateral dimensions and ultrathin thickness. These sheets attach to the fracture surfaces via planar adhesion rather than volumetric filling, enabling the formation of a continuous, stable, and dense barrier that effectively prevents fluid invasion. This "band-aid-like interfacial plugging" model represents a departure from conventional particle-stacking approaches. Moreover, the grafted PAA chains substantially enhance the dispersion stability and interfacial activity of the nanocomposite. Under harsh downhole conditions such as high temperature, high salinity, and broad pH ranges, pristine GO tends to aggregate due to charge shielding and reduction of surface functional groups. In contrast, PAA is a hydrophilic polymer rich in –COOH and –OH, which enhances hydration through hydrogen bonding with water molecules and provides steric hindrance via its flexible chains, thereby minimizing interlayer aggregation. The introduction of PAA also improves the chemical stability of GO in aqueous systems, allowing it to remain well-dispersed and suspended in water-based drilling fluids (Chen et al., 2022; Lee et al., 2024). This stable dispersion is critical for maintaining effective plugging behavior over time. More critically, the PAA chains act as molecular "adhesive tentacles," significantly enhancing the nanosheets' adhesion to fracture surfaces. These flexible chains conform to the topography of the microfractures and establish multiple contact points with the shale matrix through hydrogen bonding, electrostatic interactions, and van der Waals forces (Hu et al., 2023; Zhao et al., 2025). This multipoint interaction secures the GO-PAA at the fracture entrance, reinforcing the stability of the sealing layer. As a result, GO-PAA remains stably anchored to the fracture surface even under the high hydrostatic pressure of drilling fluid columns. Additionally, the in-plane mechanical strength of the GO nanosheets imparts excellent compressive resistance and structural integrity to the sealing layer.

In summary, GO-PAA offers a synergistic sealing mechanism that integrates the flexibility of polymeric side chains with the structural advantages of 2D nanosheets. This approach not only adapts effectively to irregular fracture morphologies but also

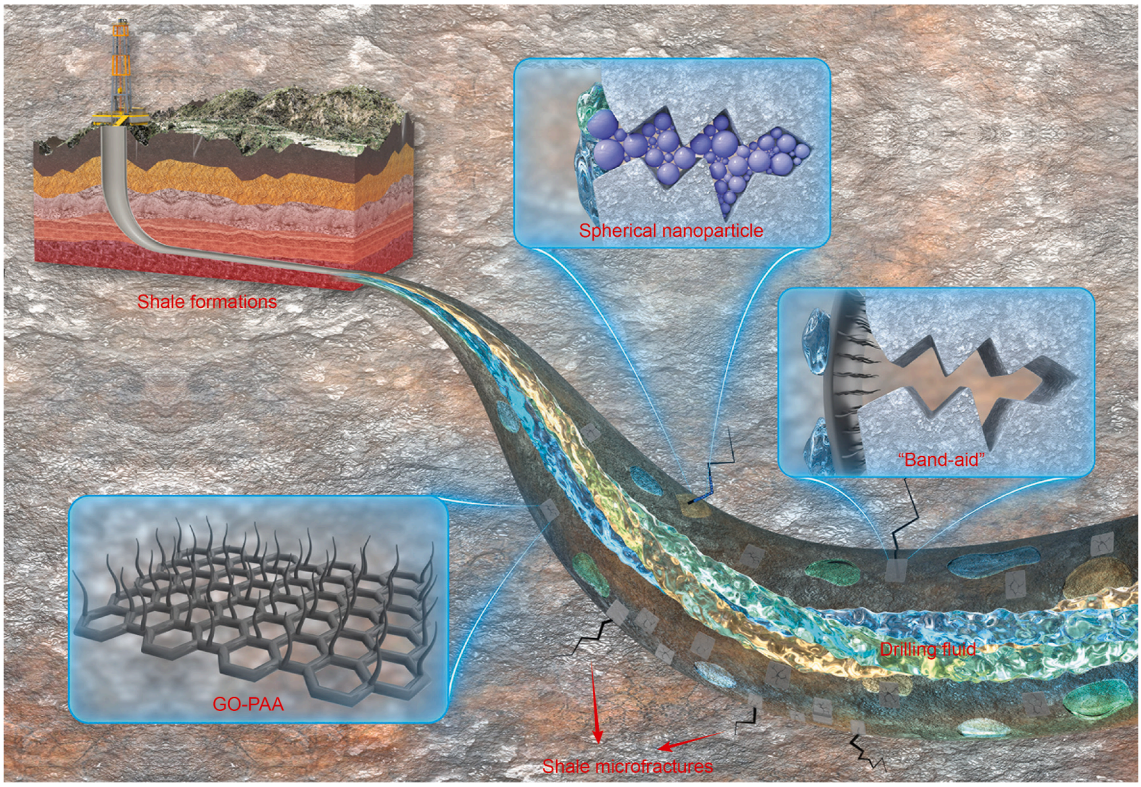

Fig. 7. Schematic diagram of the plugging of microfractures in shale formations by functionalized graphene oxide GO-PAA in drilling fluids.

reduces material consumption and enhances plugging efficiency under complex formation conditions. It represents a promising and innovative solution to wellbore instability in shale gas development.

4. Conclusions

In conclusion, we have developed a functionalized GO composite material with a simple preparation process and large-scale production feasibility. This is the first time that 2D nanomaterials have been applied in drilling fluids as efficient nanoplugging agents to address the issue of borehole instability in shale gas formations. Significant modification effects were achieved by grafting PAA polymer chains onto the surface of GO. GO-PAA exhibits excellent dispersion and stability under conditions of high salinity, high temperature, and wide pH range. Further MD simulation results indicate that the introduction of PAA side chains in the GO-PAA system enhances electrostatic repulsion and hydration effects, reduces layer bonding forces, and significantly improves dispersion stability. In terms of blocking performance, GO-PAA, through the synergistic action of its 2D sheet structure and flexible chains, forms a uniform and dense "band-aid" type plugging barrier on the surface of shale microfractures. Simulation core experiments show that the blocking efficiency of GO-PAA is significantly superior to that of traditional spherical particle plugging materials, with a permeability reduction rate of 57.53%, twice that of conventional materials. Furthermore, the modified structure of GO-PAA allows it to adapt to the irregular shapes of fractures and reduce the amount of material required. This innovative strategy successfully achieves the efficient application of 2D nanomaterials in drilling fluids, providing an effective solution to the borehole instability issue in shale gas development, and also opens up new directions for the application of 2D nanomaterials in complex formation environments.

CRediT authorship contribution statement

Dao-Xiong Li: Writing – original draft, Resources, Formal analysis. **Yang Bai:** Resources, Data curation. **Cheng Wang:** Data curation. **Na Su:** Formal analysis. **Ling-Feng Wu:** Investigation. **Deng Gu:** Investigation. **Yu-Fen Zhai:** Writing – review & editing. **Ping-Ya Luo:** Supervision, Project administration.

Data availability

Data will be made available on request.

Declaration of competing interest

We declare that we have no financial or personal relationships with others or organizations that can inappropriately influence our work. No professional or other personal interest in any product, service, or company could be construed as affecting the position presented in, or the review of, the manuscript entitled.

Acknowledgments

The work was supported by the Open Fund of State Key Laboratory of Oil and Gas Reservoir Geology and Exploitation [PLN202413], the National Natural Science Foundation of China (52274008), the National Key R&D Projects (2019YFA0708303), and the Science and Technology Cooperation Project of the CNPC-SWPU Innovation Alliance (2020CX040102, 2020CX040201).

Appendix A. Supplementary data

Supplementary data to this article can be found online at https://doi.org/10.1016/j.petsci.2025.09.030.

References

Abdullah, A.H., Ridha, S., Mohshim, D.F., Yusuf, M., Kamyab, H., Krishna, S., Maoinser, M.A., 2022. A comprehensive review of nanoparticles: Effect on water-based drilling fluids and wellbore stability. Chemosphere 308, 1–17. https://doi.org/10.1016/j.chemosphere.2022.136274.

Almarzooqi, K., Burton, N.D., Tsui, T.Y., Elkamel, A., Pope, M.A., 2024. Metal cation crosslinked, partially reduced graphene oxide membranes with enhanced stability for high salinity, produced water treatment by pervaporative separation. Nanotechnology 35, 305606. https://doi.org/10.1088/1361-6528/ad41e8.

An, Y.X., Jiang, G.C., Qi, Y.R., Ge, Q.Y., Zhang, L.Y., 2016. Nano-fluid loss agent based on an acrylamide based copolymer "grafted" on a modified silica surface. RSC Adv. 6, 17246–17255. https://doi.org/10.1039/c5ra24686e.

An, Y.X., Jiang, G.C., Qi, Y.R., Ge, Q.Y., Zhang, L.Y., Ren, Y.J., 2023. Synthesis of nanoplugging agent based on AM/AMPS/NVP terpolymer. J. Pet. Sci. Eng. 135, 505–514. https://doi.org/10.1016/j.petrol.2015.10.014.

Armor, J.N., 2013. Emerging importance of shale gas to both the energy & chemicals landscape. J. Energy Chem. 22, 21–26. https://doi.org/10.1016/S2095-4956(13)60002-9.

Arun, K.M., Mohamed, I.K.B., Shanmugam, M., Balwinder, R., Junghwan, K., 2024. Recent advances in two-dimensional nanomaterials for healthcare monitoring. ACS Sens. 9, 1706–1734. https://doi.org/10.1021/acssensors.4c00015.

Asma, N.E.H.S., Hichem, T., Mohammed, K., Mohammed, A.B., Benalia, K., Amel, H. H.B., Toumi, S., Abdeltif, A., Ali, I., Lotfi, M., 2021. Comparative investigation of the effect of eggshell powder and calcium carbonate as additivesin eco-friendly polymer drilling fluids. Sustainability 15, 3375. https://doi.org/10.3390/su15043375.

Bai, X.D., Yong, X.M., Koutsos, V., Deng, L.C., Li, K., Zhou, Y., Luo, Y.M., 2024. Dispersive and filter loss performance of calcium carbonate nanoparticles in water for drilling fluid applications. Nanotechnology 32, 1–8. https://doi.org/10.1088/1361-6528/ac1dd2.

Bhattacharjee, S., 2016. DLS and zeta potential–What they are and what they are not? J. Contr. Release 235, 337–351. https://doi.org/10.1016/j.jconrel.2016.06.017.

Cai, J., Chenevert, M.E., Sharma, M.M., Friedheim, J., 2012. Drilling and completion fluids-decreasing water invasion into Atoka shale using nonmodified silica nanoparticles. SPE Drill. Complet. 27, 103–112. https://doi.org/10.2118/146979-PA.

Cao, Z.J., Quintano, V., Joshi, R., 2024. Covalent functionalization of graphene oxide. Carbon 218, 118659. https://doi.org/10.1016/j.carbon.2023.118659.

Chen, K.F., Yang, R., Bao, H.Y., Dong, T., Jia, A., Hu, Q.H., Guo, X.W., He, S., 2023. Depositional-diagenetic process and their implications for pore development of Wufeng-Longmaxi shales in the Jiangdong block, Fuling shale gas field, SW China. Mar. Petrol. Geol. 151, 106177. https://doi.org/10.1016/j.marpetgeo.2023.106177.

Chen, Q., Guo, Z.X., Cheng, F., Chai, G.B., Li, Y.C., Luan, Y.B., Liang, J.G., 2022. Effect of GO agglomeration on the mechanical properties of graphene oxide and nylon 66 composites and micromechanical analysis. Polym. Compos. 43, 1. https://doi.org/10.1002/pc.27006.

Hu, B.W., Ren, Y.J., Sun, R., Wang, S.C., Su, S.J., 2024. Heterogeneity properties and permeability of shale matrix at nano-scale and micron-scale. Phys. Fluids 36, 096613. https://doi.org/10.1063/5.0223200.

Hu, Y.C., Peng, Q.H., Jin, T.X., Ren, G.Y., Liu, Z.R., Qian, Y., 2023. Effective adsorption of thorium ion by novel self-crosslinking polyamide acid-grafted magnetic nanocomposites. Colloids Surf., A 676, 132279. https://doi.org/10.1016/j.colsurfa.2023.132279.

Huang, X.B., Sun, J.S., Lv, K.H., Liu, J.P., Shen, H.K., Zhang, F., 2018. Application of core-shell structural acrylic resin/nano-SiO_2 composite in water based drilling fluid to plug shale pores. J. Nat. Gas Sci. Eng. 55, 418–425. https://doi.org/10.1016/j.jngse.2018.05.023.

Huang, X.B., Sun, J.S., Huang, Y., Yan, B.C., Dong, X.D., Liu, F., Wang, R., 2023. Laponite: A promising nanomaterial to formulate high-performance water-based drilling fluids. Pet. Sci. 18, 579–590. https://doi.org/10.1007/s12182-020-00516-z.

Jain, R., Mahto, V., Sharma, V.P., 2015. Evaluation of polyacrylamide-grafted-polyethylene glycol/silica nanocomposite as potential additive in water based drilling mud for reactive shale formation. J. Nat. Gas Sci. Eng. 26, 526–537. https://doi.org/10.1016/j.jngse.2015.06.051.

Jiang, G.C., Sun, J.S., He, Y.B., Cui, K.X., Dong, T.F., Yang, L.L., Yang, X.K., Wang, X.X., 2021. Novel water-based drilling and completion fluid technology to improve wellbore quality during drilling and protect unconventional reservoirs. Engineering 18, 129–142. https://doi.org/10.1016/j.eng.2021.11.014.

Jiříčková, A., Jankovsky, O., Sofer, Z.B., Sedmidubský, D., 2022. Synthesis and applications of graphene oxide. Materials 15, 920. https://doi.org/10.3390/ma15030920.

Lee, Y.S., Kim, N.R., Park, S.K., Ko, Y., Shin, Y., 2024. Effects of high-temperature thermal reduction on thermal conductivity of reduced graphene oxide

polymer composites. Appl. Surf. Sci. 650, 159140. https://doi.org/10.1016/j.apsusc.2023.159140.
Li, G.H., Niu, M.M., Huang, J., 2022. Evolution of energy systems: Patterns and mechanisms. Energy Strategy Rev. 50, 101200. https://doi.org/10.1016/j.esr.2023.101200.
Li, L., Wu, F., Cao, Y.Y., Cheng, F., Wang, D.L., Li, H.Z., Yu, Z.Q., You, J., 2024. Sustainable development index of shale gas exploitation in China, the UK, and the US. Environ. Sci. Ecotechnol. 12, 100202. https://doi.org/10.1016/j.ese.2022.100202.
Liu, J.Y., Qiu, Z.S., Huang, W.A., 2015. Novel latex particles and aluminum complexes as potential shale stabilizers in water-based drilling fluids. J. Pet. Sci. Eng. 135, 433–441. https://doi.org/10.1016/j.petrol.2015.10.003.
Liu, X.Y., Li, M.C., Liao, B., Liu, S.L., Lv, K.H., Sun, J.S., Liu, C.Z., Mei, C.T., Wu, Q.L., Lu, K.Z., 2023. Wood-derived lignocellulose nanomaterials as multifunctional agents in eco-friendly pickering emulsion-based drilling fluids. Chem. Eng. J. 475, 146372. https://doi.org/10.1016/j.cej.2023.146372.
Ma, L., Hamidinejad, M., Zhao, B., Liang, C.Y., Park, C.B., 2022. Layered foam/film polymer nanocomposites with highly efficient EMI shielding properties and ultralow reflection. Nano-Micro Lett. 14, 307–324. https://doi.org/10.1007/s40820-021-00759-4.
Melikoglu, M., 2014. Shale gas: Analysis of its role in the global energy market. Renew. Sustain. Energy Rev. 37, 460–468. https://doi.org/10.1016/j.rser.2014.05.002.
Moslemizadeh, A., Shadizadeh, S.R., 2015. Minimizing water invasion into Kazhdumi shale using nanoparticles. Iran. J. Oil Gas Sci. Technol. 4, 15–32. https://doi.org/10.22050/ijogst.2016.12475.
Novoselov, K.S., Geim, A.K., Morozov, S.V., Jiang, D., Zhang, Y., Dubonos, S.V., Grigorieva, I.V., Firsov, A.A., 2004. Electric field effect in atomically thin carbon films. Science 22, 21–26. https://doi.org/10.1126/science.110289.
Pandey, U., Sharma, C., 2024. Comparative study of graphene oxide-multifunctional oxide doping on corrosion resistance of electrodeposited nickel coatings in saline environments. Int. J. Hydrogen Energy 60, 165–179. https://doi.org/10.1016/j.ijhydene.2024.02.187.
Pedico, A., Molino, D., Zaccagnini, P., Bocchini, S., Bertana, V., Lamberti, A., 2024. Asymmetric CapMix device exploiting functionalized graphene oxide and SPEEK coatings for improved energy harvesting from salinity gradients. Adv. Sustain. Syst. 8, 2400106. https://doi.org/10.1002/adsu.202400106.
Safaei, S., Tavakoli, R., 2017. On the design of graphene oxide nanosheets membranes for water desalination. Desalination 422, 83–90. https://doi.org/10.1016/j.desal.2017.08.013.
Sawada, H., Nogami, C., 2004. Capillary electrophoresis-electrospray ionization mass spectrometry using uncoated fused-silica capillaries and alkaline buffer solution for the analysis of small carboxylic acids. Anal. Chim. Acta 507, 195–202. https://doi.org/10.1016/j.aca.2003.11.047.
Tang, Z.Q., Souza, F.B.d., Sagoe-Crentsil, K., Duan, W.H., 2024. Enhancing geopolymer performance with silane-functionalized graphene oxide: Efflorescence reduction, pore refinement, and improved high-temperature properties. Constr. Build. Mater. 440, 137420. https://doi.org/10.1016/j.conbuildmat.2024.137420.
Toscano, A., Bilotti, F., Asdrubali, F., Guattari, C., Evangelisti, L., Basilicata, C., 2016. Recent trends in the world gas market: Economical, geopolitical and environmental aspects. Sustainability 8, 154. https://doi.org/10.3390/su8020154.
Verma, A., Yadav, B.C., 2024. Comprehensive review on two dimensional nanomaterials for optical biosensors: Present progress and outlook. Sustain. Mater. Technol. 40, e00900. https://doi.org/10.1016/j.susmat.2024.e00900.
Wang, D.N., Dou, Y., Zhang, X., Bi, K., Panneerselvam, I.R., Sun, H.F., Jiang, X.Y., Dai, R., Song, K.N., Zhuang, H.L., Lu, Y.F., Wang, Y., Liao, Y.L., Ding, L., Nian, Q., 2024. Manufacturing and applications of multi-functional holey two-dimensional nanomaterials–A review. Nano Today 55, 102162. https://doi.org/10.1016/j.nantod.2024.102162.
Wei, J.G., Li, J.T., Zhang, A., Shang, D.M., Zhou, X.F., Niu, Y.T., 2023. Influence of shale bedding on development of microscale pores and fractures. Energy 282, 128844. https://doi.org/10.1016/j.energy.2023.128844.
Wu, Y.P., Wang, Z.H., Yan, Z., Zhang, T., Bai, Y., Wang, P.Q., Luo, P.Y., Gou, S.H., Guo, Q.P., 2017. Poly(2-acrylamide-2-methylpropanesulfonic acid)-modified SiO_2 nanoparticles for water-based muds. Ind. Eng. Chem. Res. 156, 12–24. https://doi.org/10.1021/acs.iecr.6b03450.
Xie, G., Luo, P.Y., Deng, M.Y., Wang, Z., 2015. Nanoplugging performance of hyperbranched polyamine as nanoplugging agent in oil-based drilling fluid. J. Nanomater. 2015, 1–8. https://doi.org/10.1155/2015/821910.
Yagura, K., Zhang, Y.F., Enomoto, Y., Iwata, T., 2021. Synthesis of highly thermally stable divanillic acid-derived polyamides and their mechanical properties. Polymer 228, 123907. https://doi.org/10.1016/j.polymer.2021.123907.
Yang, F., Ning, Z.F., Wang, Q., Zhang, R., Krooss, B.M., 2016. Pore structure characteristics of lower Silurian shales in the southern Sichuan Basin, China: Insights to pore development and gas storage mechanism. Int. J. Coal Geol. 156, 12–24. https://doi.org/10.1016/j.coal.2015.12.015.
Yu, Y.H., Li, W.L., Lin, W.T., Fu, P., Xu, Z.K., Wan, L.S., 2024. High permeance polyamide nanofiltration membranes based on poly(l-lactic acid) electrospun nanofibrous membranes with controlled hydrophilicity. ACS Appl. Nano Mater. 7, 12003–12014. https://doi.org/10.1021/acsanm.4c01635.
Zhang, J.J., Zhang, J.S., Miao, P., Shu, Y.H., 2024. Experimental investigation and analysis of the impact of salinity erosion on the strength of graphene oxide cement soil. Case Stud. Constr. Mater. 21, e03413. https://doi.org/10.1016/j.cscm.2024.e03413.
Zhao, C.X., Liu, J.F., Wei, J.B., Dai, H.Y., Gao, C.Y., Xu, H.N., Zhong, W., 2025. Velocity dependence of permeability evolution and the effect of fluid pressure heterogeneity on frictional stability of Longmaxi shale. Bull. Eng. Geol. Environ. 84, 1–14. https://doi.org/10.1007/s10064-024-04052-7.
Zhao, X., Qiu, Z.S., Wang, M.L., Xu, J.G., Huang, W.A., 2019. Experimental investigation of the effect of drilling fluid on wellbore stability in shallow unconsolidated formations in deep water. J. Pet. Sci. Eng. 175, 595–603. https://doi.org/10.1016/j.petrol.2018.12.067.
Zhou, Y., Zhong, X.Q., Nie, X., 2024. Identification and parameter characterization of pores and fractures in shales based on multi-scale digital core data. Adv. Geo-Energy Res. 13, 146–160. https://doi.org/10.46690/ager.2024.08.08.
Zou, C.E., Lin, M.J., Ma, F., Liu, H.L., Yang, Z., Zhang, G.S., Yang, Y.C., Guan, C.X., Liang, Y.B., Wang, Y., Xiong, B., Yu, H., Yu, P., 2024. Development, challenges and strategies of natural gas industry under carbon neutral target in China. Petrol. Explor. Dev. 51, 476–497. https://doi.org/10.1016/S1876-3804(24)60038-8.